Overview of the End–of–Mission Observation Experiments of Precipitation Radar onboard the

Tropical Rainfall Measuring Mission Satellite

Nobuhiro Takahashi (1), Hiroshi Hanado (2), Kenji Nakamura (3), Kaya Kanemaru (4), Katsuhiro Nakagawa (2), Toshio

Iguchi (2), Tomomi Nio (4), Takuji Kubota (4), Riko Oki (4), and Naofumi Yoshida(5)

(1) Institute for Space–Earth Environmental Research, Nagoya University

(2) National Institute of Information and Communications Technology

(3) Dokkyo University

(4) Japan Aerospace Exploration Agency

(5) Remote Sensing Technology Center of Japan

Abstract

Special experiments using the precipitation radar (PR) onboard the Tropical Rainfall Measuring Mission

satellite (TRMM) during descent after the orbital maintenance fuel was depleted are reported in this

paper.   In these special observation experiments, a 90° yaw maneuver experiment, a wide swath width

experiment, and the dense sampling experiments were carried out.   The key operation of these

experiments was a large change in the phase shifter settings of the transmitter and receiver, which was

not tested before or after the launch.   In addition, the 90° yaw experiment required the special

operation of the satellite, whereas the other two experiments were implemented by changing only the

PR operation.   During the experiments, the PR was operated and the expected data were obtained.

1

The preliminary results suggest the possibility of future radar observation from space, and the results of these experiments will be utilized as basic data to improve the algorithm of the dual-frequency precipitation radar （DPR） onboard the global precipitation measurement （GPM） mission core satellite and the design of future spaceborne precipitation radars.

1.　Introduction

The Tropical Rainfall Measuring Mission satellite (TRMM [1]) has continued its observation for more than 17 years since its launch in 1997 as a result of changing its orbital altitude from 350 km to 402.5 km in August 2001 [2] to extend its observation period.　The fuel for the orbit maintenance was finally exhausted in July 2014; since then, the satellite gradually descended and eventually reentered the atmosphere in June 2015. Although the microwave radiometer (TMI), which is one of the main sensors of the TRMM, had continued its observation during the orbital descent, the precipitation radar (PR [3]), another main sensor, cannot obtain meaningful data in the normal observation mode because of the limited vertical observation window during the orbital descent.　It was a unique opportunity to perform special observation experiments in order to use the PR efficiently during the descent, and such experiments were proposed to the mission operator (NASA).　The special experiments proposed include observation modes that were not carried out during the normal observation of the TRMM and TRMM/PR even during ground testing, and these modes are expected to contribute to improving the rain retrieval algorithm of the dual-frequency precipitation radar (DPR) onboard the global precipitation

2

measurement (GPM [4]) mission core satellite and the design of future spaceborne precipitation radars.

In this report, the outline and preliminary results of these special experiments are described.

2.   Satellite altitude and observation window of PR

Figure 1 shows the satellite altitude since July 2014.   After the descent was started in July, the

satellite returned to its original nominal altitude of 350 km in about seven months.   When the altitude

became 335 km, the passivation operation of the satellite was started to prepare for its final reentry

into the atmosphere.   The observation window of the TRMM/PR, as shown in Fig. 1 in [5], is set at a

fixed range (50 km=125 m x 400 range bins) from the satellite, and the observation data are stored in

the onboard memory of the satellite.   Because of the limitation of the onboard memory of the satellite

to be downlinked at various contact intervals, only data with a range of about 35 km with 250 m range

resolution (140 bins) from a prefixed distance for each angle bin are downlinked to the ground.   The PR

is required to obtain the data from the ground to 15 km in altitude everywhere from 35° south to 35°

north in latitude.   Since the pulse repetition frequency of the PR is fixed as 2776 Hz, then the

maximum width of the observation window is about 54 km, the satellite altitude was decided to be 402.5

km (52.5 km higher than the nominal altitude of 350 km) at the time the orbital altitude was increased in

2001 [2].   In the 402.5 km observation, the same observation as that at the nominal altitude of 350 km

is realized, except for the mismatch of the angle of transmission and the reception of one of the 32

3

averaging pulses [2].   When the satellite altitude is decreasing, the surface echo gradually moves in

the observation window and finally reaches the top of the window.   After that, the top of the rain echo

appears near the bottom of the window and then finally returns to the normal position when the

satellite altitude is 350 km.   Figure 2 shows an example of the observation (received power in dBm) at

the time of the orbital rise in 2001 (picture of the TRMM orbit viewer).   In an extreme case, an echo

from the earth's surface will appear in the top of the window, and the top of a precipitation echo is

simultaneously observed at the bottom of the window.

3.   Observation plan of PR during satellite descent

3.-1 Observation plan of PR

We decided to continue the normal observation as long as possible until the observation window

captures both the echo from the earth's surface and the rain echo of about 5 km depth during one

orbit.   The normal observation continued until October, as shown in Fig. 1, about three months after

the start of the descent of the satellite in July 2014.   Note that, under the normal observation

criterion, the observation window covers the 5 km range above the ground including the echo from the

earth's surface, the rain profile retrieval algorithm (level 2A25 [6][7]) and relating algorithms (Level

2A21 and 2A23 [8][9][10]) work without breakdown, and the total amounts of attenuation are covered

mostly below this altitude (bright band height and below) for meaningful attenuation correction in 2A25

4

algorithm.   When the observation window did not satisfy the criterion, three special experiments (wide swath, 90° yaw and dense sampling) were conducted as indicated in Fig. 1.   The details will be given in the following section.

Since the TRMM/PR performs electronic scanning in which the beam direction (transmission and reception) is determined by adjusting the phase shifts of 128 slotted waveguide antennas and the PR has 400 equidistant range bin samples for each angle bin (equivalent to a 50 km window), there are some degrees of freedom for choosing the scan angle and downlink data.   In particular, a scan angle wider than the normal scan angle is advantageous for catching the rain echo, as shown in Fig 3, because the distance between the satellite and the rain echo (or the earth's surface) is larger for a wider scan angle.   Note that the scan angle is not so large for the effect of the grating lobe that is supposed to appear the angle of about −60 degrees when the scan angle is +30 degrees.   The PR completes one scan that consists of 49 angle bin observations in 0.6 s.   Since the footprint size is designed to be equivalent to the satellite movement in one scan (4.3 km), the scan angle intervals are also designed to be equivalent to the footprint size that corresponds to a 0.71° scan angle (at the satellite altitude of 350 km).   For the special experiments, the scan angles of 49 angle bins were modified.   Therefore, gaps may appear between the successive footprints upon changing the scan angles for a wider scan angle experiment.   Dense sampling observation limits the interval between scanning angles to 1/3 or 1/4 and limits the number of angles from 12 to about 15 to realize dense sampling for both the

5

along–track and cross–track directions.

Note that owing to the malfunction of the satellite battery, electric power cannot be supplied to PR's

observation equipment when the solar beta angle (the angle between the projection of the solar vector

and the satellite orbit circle) is between +/− 20°.   The PR observation was therefore limited to only the

sunny side of the orbit during that periods (October 27 to November 13, 2014, December 5 to

December 27, 2014, January 21 to February 14, 2015, and March 5 to March 12, 2015).

The originally proposed PR experiments during the descent included the following experiments in

addition to the three actually performed experiments: (1) radiometer mode observation to realize a

radiometer–like observation by turning off the transmission of the PR, (2) KaPR emulation observation

with the same footprint arrangement as the KaPR of the GPM core satellite, and (3) a pitch maneuver in

order to check the clutter effect by changing the pitch angle of the satellite.   These experiments were

excluded for the following reasons: Regarding (1), we planned to integrate all the range bin data   to

obtain a very precise noise level to be like a radiometer.   Since most of the rain echoes are out of the

observation window, it is concluded that sufficient data that are not contaminated by rain echoes are

available without turning off the PR.   Regarding (2), it can be covered by the dense sampling

experiment explained in Section. 4–4.   Regarding (3), it has already been implemented by GPM/DPR in

orbit with the same purpose.   Table 1 summarizes the experimental periods and SMA (semi–major

axis)   satellite altitudes (it is difference between satellite semi–major axis and the average earth radius,

6

so this number is different from the actual distance between the earth's surface to the satellite) during

the special experiments. In addition, Table 2 summarizes the orbit numbers for the 90° yaw maneuver

experiment. In Table 1, three types of wide swath experiments were performed to adjust the

observation window for the rain observation according to the satellite altitude. In this case, wider

swath setting (like as wide swath #3) is available as the satellite descent from the nominal altitude (see

also Fig. 3). Figure 4 shows the geometric positions of the footprints of three wide-scan experiments.

In this figure, the scan geometries of both the 90° yaw experiment and the dense sampling experiment

are also shown. During the 90 ° yaw experiment, cross-track direction must be read along-track

direction in this figure.

Other than the special experiments, a check-out activity for PR was implemented just before the

passivation of the PR at the satellite altitude of 340 km. The primary purpose of this check-out was

to confirm the status of the frequency converter and intermediate frequency (FCIF) unit and the

system control and data processing (SCDP) unit, which were switched to the redundant system in 2008.

In this experiment, both units were switched to the primary side.

3-2. Data processing

Data during the satellite descent are considerably different from the normal observation data because

of the different data acquisition range bins and scan angles. In addition, the onboard surface detection

algorithm [3] did not work properly because this algorithm was developed under the assumption that

7

the surface echo exists within the sampling range. Thus, the range oversampling data for the surface

are not from a suitable range of data. In the same manner, the system noise data, which are assumed

to be sampled in precipitation-free ranges, may be contaminated by the echoes from precipitation and

the earth's surface. Therefore, several parameters such as noise level, surface peak range bin,

over-sample data that are required for level 1 processing cannot be calculated. Furthermore, since

data acquisition range bins and scan angles were different from those in the normal observation, a

major modification of the level 1 algorithm is needed. JAXA improved the level 1 algorithm to produce

correct incidence angle information and geophysical footprint positions, which are essential for data

analysis. The high-level algorithms were implemented only for the normal observation mode and

dense sampling observation. The level 2 algorithms do not work properly because the sigma zero

estimation algorithm requires the spatial continuity of sigma zero, and the bright-band detection

algorithm is not applicable for wider scan angles owing to similar problems in the level 1 product as

mentioned above. In addition, it is impossible to verify the quality of all the experimental data. For

the path integrated attenuation (PIA) that is used for the attenuation correction of the rain profile if it

is larger than a threshold. Since the method uses both the previous no-rain footprint scans of the

same incident angle (spatial reference) and the database containing past data (temporal reference)

[8][9], PIA was not correctly estimated during the wide-swath experiment, particularly in the temporal

reference cases. Similarly, since the bright band detection algorithm assumes a bright band profile

8

with prefixed incidence angles [10], the exact bright band detection algorithm may fail.

The spacecraft itself may have problems during its descent. Figure 5 shows the differences in the range distance from the radar between the −11° incident angle and the +11° incident angle with the same manner as [11]. If the roll angle control of the spacecraft is correct, the difference is zero (the PR points normal to the earth's surface). This figure indicates the sinusoidal change (see the fitted sinusoidal curve in Fig. 5) in one orbit and that the amplitude is about 2 range bins (0.5 km), indicating a roll angle error of about 0.2°. The reason of the error in the roll angle is not clear now. We also have to evaluate the excess error of the pitch angle control, but this is very difficult to verify from the observation data. Since these pitch and roll errors are not appear in the satellite attitude data, careful treatment of the data during the analysis, such as the calculation of surface scattering cross section and even the geolocation of a footprint, is needed.

4.　Overview of experiments and initial observation results

4-1. Normal observation mode

The normal observation mode was continued when the satellite altitude was from 402.5 to 392.5 km (from July 16 to October 6, 2014) and 360 to 340 km (from February 10 to March 20, 2015). In these altitude ranges, the precipitation echo could be obtained from the earth's surface to an altitude of about 5 km (observation up to 0 ℃ altitude), and we also considered that the rain profile retrieval

9

algorithm (level 2A25 [6][7]) can work with better accuracy if the echo depth is larger than 5 km to include information from the earth's surface. Note that the remaining fuel was consumed at the altitude of 350 km to maintain the normal observation as long as possible. The estimated precipitation profile in the case that the observation window of rain is about 5 km must be verified because this approach assumes the effects above the melting layer on the rain profile retrieval and the path integrated attenuation are negligible. A possible way to verify is to use the GPM/DPR data by using the coincident observation data and/or by statistical way (e.g. area average rainfall amount).

4-2. 90° yaw maneuver observation

This observation mode was realized to rotate the satellite yaw direction by 90°, then the PR scans in the along-track direction and acquires the data from various incidence angles. The primary targets of this experiments were to obtain the incidence angle dependences of the earth's-surface-normalized scattering cross section (sigma zero) and the melting layer (bright band) and the changes in the rain structure using the time difference (maximum of about 1 min) of the observation. To avoid the risks associated with satellite operation, this operation was implemented only when the satellite was flying on the sunny side and during the operator's working time. Thus, the observation was confined to about 20 min for each orbit and to four orbits a day. The total observation time was 880 min (20 min × 4 times a day x 11 days) from November 15 to 25, 2014. The operation mode of the PR was set as the wide-swath observation because of the optimization of the sampling window with the satellite altitude. Then the PR's scan changed cross-track direction to along-track direction and returned to cross-track direction in one orbit during the 90° yaw experiment. Note that nadir observation was included in the angle bin setting of this mode. The observation of the TMI was changed to perform the

10

conical scan on the right−hand side (or left−hand side) of the flight direction during this experiment.

Figure 6 shows an example of observed echoes during this experiment. The interval between the successive images is eight scan (about 5 second intervals, duration is about 15 seconds).   Note that the only received power (in dBm) information from level 1 (1B21) data are available during the 90° yaw maneuver observation and wide swath observation because the system noise data were not verified enough to calculate the radar reflectivity factor (Z).   Since the PR scans along−track direction and the flying speed of the satellite relative to the ground was about 7.2 km/s, echoes moved from the right to the left in this figure without changing the structure.   Figure 6 indicates the echo structure is not perfectly the same even the 5 second intervals.   This is because the observation location was not the same but slightly shifts as explained in the next paragraph.

Although the objective of this experiment was to observe a rain system from various incidence angles, the trajectory of the PR's footprint shifted to the west owing to the rotation of the earth near the equator (Fig. 7).   In this figure, the scan trajectory of scan number 407 shifted about 7 km from that of scan number 387.   Since the comparison of rain structures from various incident angles was the objective of this experiment, the shift of the location was a serious problem for the analysis.   Figure 8 shows the shift from the start of the scan (angle bin 0 = +17° incident angle) to the end of the scan (angle bin 48 = −17° incident angle) as the extreme case.   This figure indicates that the comparison of the large incident angle from the opposite direction is not possible near the equator because the footprint center shifts about 10 km.   On the other hand, this effect is small at the north or south edges (i.e., 35° north and south) because the satellite flies relatively parallel to the latitude lines.   Moreover, the geometric scanning pattern of the PR clearly appeared during this 90° yaw experiment.   Since the antenna of the PR was physically tilted by 4° from the nadir along−track direction and the electrical beam center was set to the nadir (that is, the electric axis is the nadir), the scan of the PR is slightly conical, and this experiment clearly reveals the scan geometry shown in Fig. 9 as an example of the footprint trajectory around 35° south.   In this figure, the ordinate (latitude range) is magnified to 0.06°,

11

whereas the abscissa (longitude range) is set to 5°, indicating that the footprint trajectory is shifted by about 5 km from the case of linear scanning.

4-3. Wide-swath observation

The primary purpose of this experiment was to acquire data for future spaceborne radars with a wide-swath observation larger than those of the TRMM/PR and GPM/DPR.   The swath width of the PR was increased by changing the phase code of its transmitter/receiver system.   The typical scan range is about +/- 17°, which corresponds to a 245 km swath width at 400 km altitude; one swath consists of 49 angle bins.   In contrast to the TMI (with a swath width of about 800 km), the swath width of the PR is too small for global precipitation sampling and a wide-swath observation is desired to increase coverage.   In this wide-swath experiment, the scan angle settings werere optimized to maximize the precipitation echo sampling according to the satellite altitude with the constraints of the 49 angle bins in one swath, the onboard data sampling range, and the downlink data capacity of each angle bin. This experiment was conducted from October 27, 2014 to January 4, 2015, except during the 90° yaw experiment.   In order to optimize the precipitation measurement according to the change in the satellite altitude, three sets of phase code were prepared.   Figure 10 shows the vertical cross section of the echo at the time of the first experiment (WS1).   In this case, the swath width was about 370 km. The nadir beam is included in this scan setting, and the data interval near the nadir direction is sparse.   The preliminary result in this experiment shows that the main-lobe clutter depth that is caused by the slanted incident angle of the beam increases for a larger incident angle, whereas sigma zero at the wide scan angle becomes small as expected, indicating the possibility of distinguishing a precipitation echo in the main-lobe clutter range even near the earth's surface.   Figure 11 shows the surface echo profile with the local zenith angle from 18.75° to 30.13° during the WS2 experiment on November 25, 2014.   The local zenith angle of 18.75° (the top line) corresponds to the scan edge of the normal observation mode.   In this figure, the profile of the 30.13° local zenith angle is about 25 dB

12

smaller than that of the 18.75° profile and it is about 15 dB higher than the noise level. The clutter range of this widest case (30.13° local zenith angle) expanded by about 5 bins (x 250 m = 1.25 km) from the scan edge of the normal observation (local zenith angle of 18.75°) by comparing the range bin to be the noise level. It is correcponds to the simple estimation of tilted beam with the footprint size (3 dB beam width) of 5 km. This result indicates the applicability of the wide-scan data for precipitation observation; contamination of the ground clutter can be removed to some extent if the precipitation is relatively higher than the noise level. Figure 12 shows examples of comparisons between the actual cases of rain and no rain in the same orbit as that in Fig. 11 for relatively wide scan data. The top right frame in Fig. 12 (local zenith angle is 18.0°) corresponds to the scan edge profile of normal observation as the reference. Although the expected clutter range increases from the local zenith angle of 18.0° to about 1.25 km atthe scan edge(left bottom in Fig. 12, local zenith angle is 30.2°), the rain echo can be distinguished at altitudes lower than the clutter top comparable to the case of the local zenith angle of 18.0° if the rain echo is higher than about 30 dBZ. Concerning the use of the wide-scan data, since the incident angle is more than 30° at the edge of the scan, the line-of-sight profile cannot represent the vertical profile observation and careful treatment is required.

4-4. Dense sampling observation

The purpose of this experiment was to see how the detailed structure of precipitation can be seen spatially, i.e., dense sampling data, or in other words, oversampling data, without changing the footprint size in order to verify the KaPR onboard the GPM core satellite and to obtain data for designing future spaceborne radars. Since the footprint size and spacing is about 5 km for TRMM/PR and GPM/DPR, it is too large to see the detailed sturcture of a single convective cloud which horizontal scale is typically about 10 km. This large footprint size causes serious non-uniform beam filling effect that is one of the important item for the DPR algorithm development. So this experiment is also expected to provide the information of non-uniform beam filling effect.

13

The experiment was implemented with 3- to 4-fold denser footprint spacing than in the normal observation. This was realized by changing the phase code in the same manner as in the wide-swath experiment. Figure 13 shows the footprint locations of this experiment. As explained above, the intervals between footprint centers are 1/3 (or 1/4) of those in the normal observation in both the flight direction and scanning direction. An example of the vertical profile of the along-track direction is shown in Fig. 14. In this figure, a simulated normal observation profile obtained by thinning out the data is shown for comparison. In other words, the dense data is simply sampled at footprint location equivalent to those found in normal observations and no interpolation is applied. This figure suggests that the spatial oversampling may give a more detailed structure of precipitation. For example, the rain streak right of the 2260 tick mark is smooth in the dense sampling data (bottom), whereas a steplike structure appeared in the normal sampling simulation (top).

5. Conclusions

In this report, we gave an overview of the special experiments using the PR during the descent of the TRMM from 402.5 to 340 km (July 2014 to March 2015). Since the PR cannot obtain high-quality data during the descent, special experiments that are not possible during the normal observation period were carried out. The main activity was to observe the change in the scan pattern of the PR under a limited degree of freedom of the PR operation. In these experiments, the capability of the spaceborne precipitation radar for obtaining the fine structure of precipitation in the case of a very large swath width and very dense sampling was demonstrated by the actual radar in orbit. Furthermore, we obtained the data during the 90° yaw operation of the satellite, which was not allowed during the normal observation period. Detailed analysis will be carried out for each experiment, and the results obtained from these experiments will be useful for future precipitation observation missions from space. In particular, the initial results of observation with a large scan width and dense sampling show the possibility of upgrading the precipitation observation through a major change in the current spaceborne

14

precipitation radar design.

Acknowledgements

References

[1] J. Simpson, J., R. E. Adler, and G. R. North, 1988: A proposed Tropical Rainfall Measuring Mission (TRMM) satellite, Bull Am. Meteorol. Soc., 69, 278–295.

[2] N. Takahashi and T. Iguchi, 2004: Estimation and correction of beam mismatch of the precipitation radar after an orbit boost of the tropical rainfall measuring mission satellite, IEEE Trans. Geosci. Remote Sens., 42, 2362–2369.

[3] T. Kozu, T. Kawanishi, H. Kuroiwa, M. Kojima, K. Oikawa, H. Kumagai, K. Okamoto, M. Okumura, H. Nakatsuka and K. Nishikawa, 2001: Development of precipitation radar onboard the tropical rainfall measuring mission satellite. IEEE Geosci. Remote Sens., 39 (1), 102–116.

[4] A. Y. Hou, Kakar, R. K., Neeck, S., Azarbarzin, A. A., Kummerow, C.D., Kojima, M., Oki, R., Nakamura, K., and Iguchi, T, 2014: The global precipitation measurement mission, Bull. Am. Meteo.. Soc., 95, 701–722.

[5] N. Takahashi, H. Hanado and T. Iguchi, 2006: Estimation of path-integrated attenuation and its non-uniformity from TRMM/PR range profile data, IEEE Trans. Geosci. Remote Sens., 44, 3276–3283.

[6] T. Iguchi, T. Kozu, J. Kwiatkwoski, R. Meneghini, J. Awaka, and K. Okamoto, 2009: Uncertainties in the rain profiling algorithm for the TRMM precipitation radar. J. Meteoro. Soc. Japan., 87A, 1–30.

[7] T. Iguchi, T. Kozu, R. Meneghine, J. Awaka, and K. Okamoto, 2000: Rain-profiling algorithm for the TRMM precipitation radar, J. Appl. Meteorol., 39, 2038–2052.

15

[8] R. Meneghini, J. A. Jones, T. Iguchi, K. Okamoto, and J. Kwiatkowski, 2004: A Hybrid Surface

Reference Technique and Its Application to the TRMM Precipitation Radar, J. Atmos. Oceanic Technol.,

21, 1645–1658.

[9] R. Meneghini, T. Iguchi, T. Kozu, L. Liao, K. Okamoto, J. A. Jones, and J. Kwiatkowski, 2000: Use of

the surface reference technique for path attenuation estimates from the TRMM Precipitation Radar. J.

Appl. Meteorol., 39, 2053–2070.

[10] J. Awaka, T. Iguchi and K. Okamoto, 2009: TRMM PR Standard Algorithm 2A23 and its

Performance on Bright Band Detection, J. Meteor. Soc. Japan, 87A, 31–52.

[11] J. Kwiatkowski, Stout, J.; Bilanow, S., 2002: Estimating TRMM spacecraft attitude errors using the

precipitation radar, Geoscience and Remote Sensing Symposium, 2002. IGARSS '02. 2002 IEEE

International, vol.1, no., pp.287,289 vol.1, 2002 doi: 10.1109/IGARSS.2002.1025015

16

Tables

Table 1. Summary of the special experiment of the precipitation radar during the TRMM descent			
Experiment/events	Duration	Orbit number	SMA (semi major axis) satellite altitude range
Normal observation	2014/7/16 – 2014/10/7*	#93230	392.0 km
Wide swath #1	2014/10/27–2014/11/15	#96537 – #96832	387.3 km – 382.5 km
90º yaw maneuver	2014/11/15–2014/11/25**	#96833 – #96993	382.5 km – 379.8 km
Wide swath #2	2014/11/24–2014/12/17	#96978 – #97333	379.8 km – 373.4 km
Wide swath #3	2014/12/17–2015/1/5	#97334 – #97634	373.4 km – 366.8 km
Dense sampling #1	2015/1/5–2015/1/24	#97635 – #97914	366.8 km – 361.9 km
Dense sampling #2	2015/1/24–2015/2/12	#97915 – #98231	361.9 km – 355.7 km
Normal observation	2015/2/12–2015/3/31	#98231 – #98987	355.7 km – 340.0 km
Instrument checkout	2015/4/1		340.0 km
Passivation of PR	2015/4/8		
*: Normal processing was carried out until October 7, 2014. Normal observation was continued from October 7 to 27, 2014, but data processing was not implanted because of criteria explained in section 4-1 **: The orbit numbers for the 90º yaw experiment are shown in Table 2.			

Table 2. Orbit numbers for the 90º yaw maneuver experiment		
90º yaw maneuver	Experimental orbit number	Phase code type
Day #1 (2014/11/15)	96834 96835 96836 96837 96838	90º yaw maneuver
Day #2 (2014/11/16)	96849 96850 96851 96852 96853	90º yaw maneuver
Day #3 (2014/11/17)	96865 96866 96867 96868 96869	90º yaw maneuver
Day #4 (2014/11/18)	96880 96881 96882 96883 96884	90º yaw maneuver
Day #5 (2014/11/19)	96896 96897 96898 96899 96900	90º yaw maneuver
Day #6 (2014/11/20)	96912 96913 96914 96915 96916	90º yaw maneuver
Day #7 (2014/11/21)	96927 96928 96929 96930 96931	90º yaw maneuver

17

| Day #8 (2014/11/22) | 96944 96945 96946 96947 | 90° yaw maneuver |
Day #9 (2014/11/23)	96959 96960 96961 96962	90° yaw maneuver
Day #10 (2014/11/24)	96975 96976 96977 96878	90° yaw maneuver
Day #11 (2014/11/25)	96990 96991 96992 96993	Wide swath #2

18
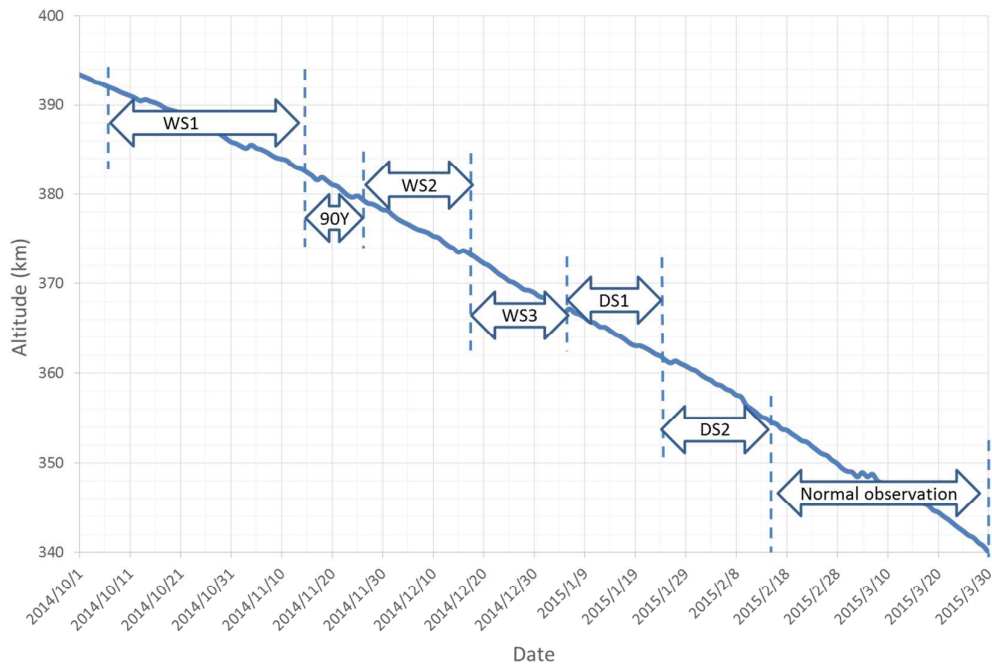
Figures

Fig. 1.　TRMM altitude prediction during the special experiment of the precipitation radar (PR).　In this figure, WS stands for the wide-swath experiment, 90Y stands for the 90° yaw maneuver experiment and DS stands for the dense sampling experiment.

19
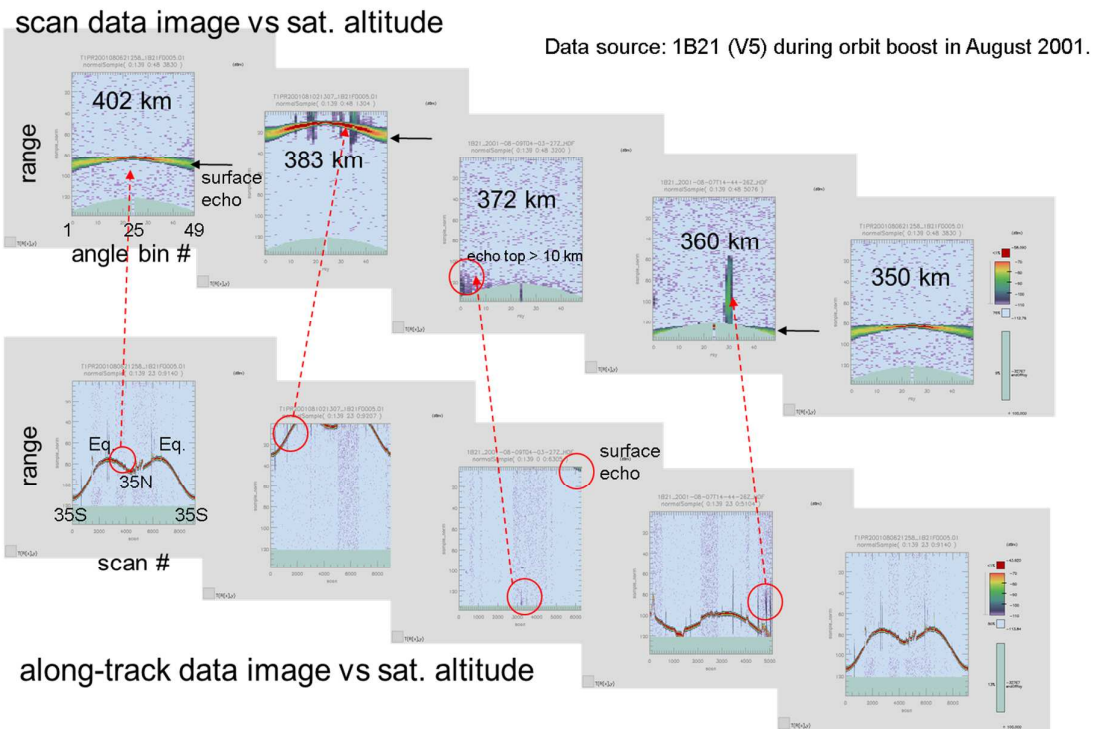
Fig. 2. Examples of vertical cross sections of normal observation (received power in dBm) by the PR when the satellite altitudes were between 350 and 402 km. The bottom five panels are samples of along-track profiles of the nadir incident angle for one granule and the top five panels are examples of cross-track profiles in the area designated by red circles in the along-track profiles. Data were taken during the orbit boost in August 2001.

20
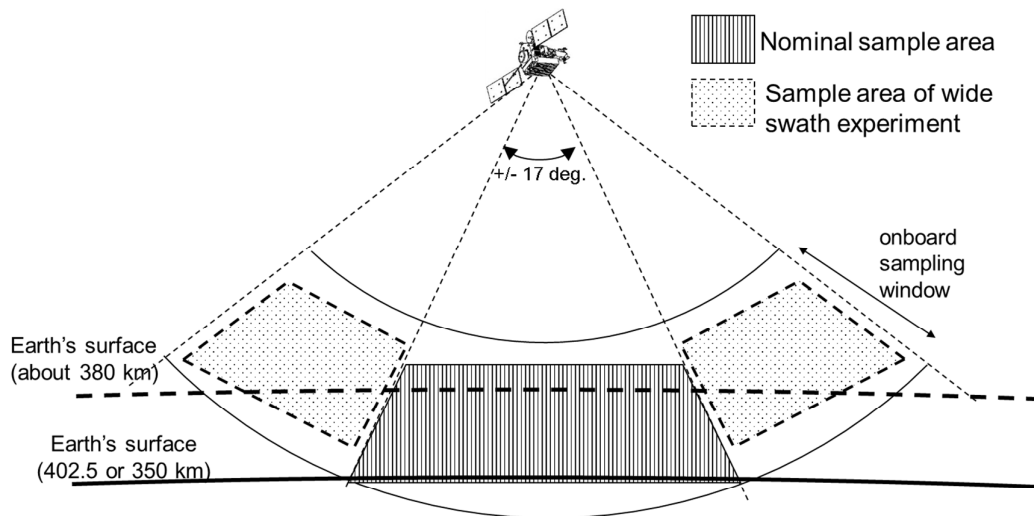
Fig. 3. Schematic illustration of cross-track scan geometry of TRMM PR nominal satellite altitude (402.5 and 350 km) with normal observation (the hatched area is the sampling range) and the special experiment satellite altitude (e.g., 380 km) in the wide-swath experiment (the dotted area is the sampling range).

21
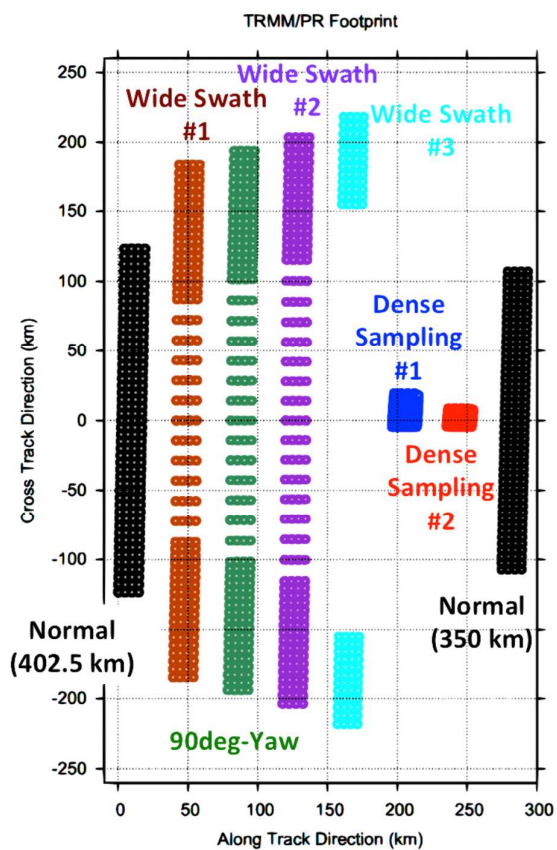
Fig. 4.   Scan geometry of the special experiment of TRMM/PR.   The detailed scan geometry of the dense sampling is shown in Figure 13.   Note that cross-rack direction must be read along-track direction during the 90 degree yaw experiment.

22

20141125.96985 angle bin 18 − 31
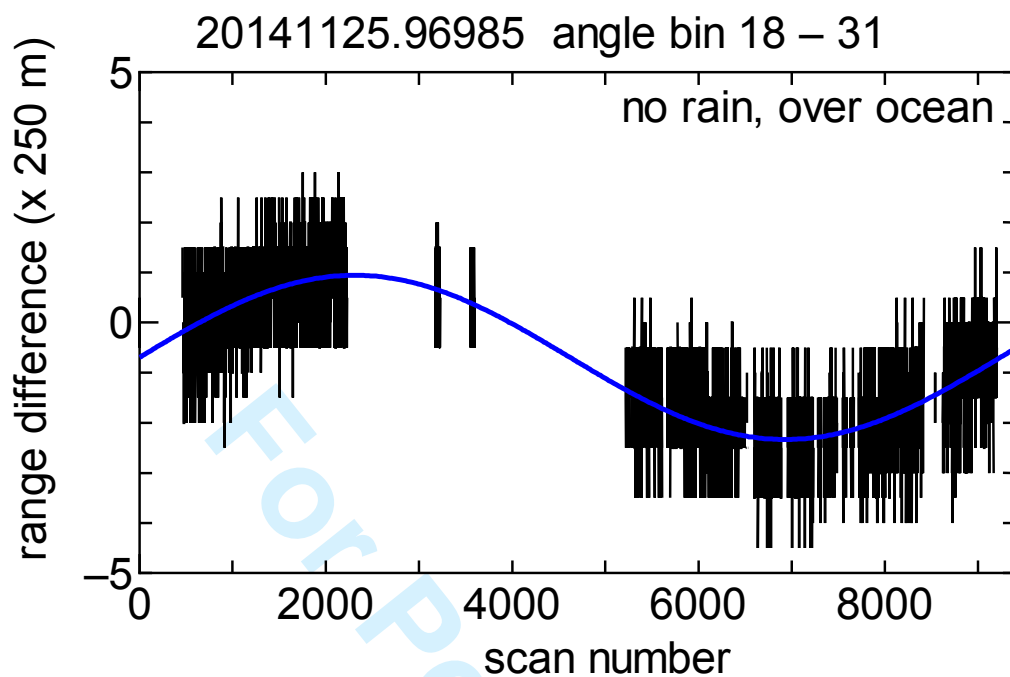
Fig. 5. Difference in range from the satellite to the surface between the same local zenith angles with opposite directions (angle bin 18: +11° local zenith angle and angle bin 31: −11° local zenith angle) during one orbit. Solid curve indicates a fitted sinusoidal curve to the range difference data for one orbit. One bin corresponds to 0.25 km. Note that only "no rain, over ocean" data are used for the analysis.

23
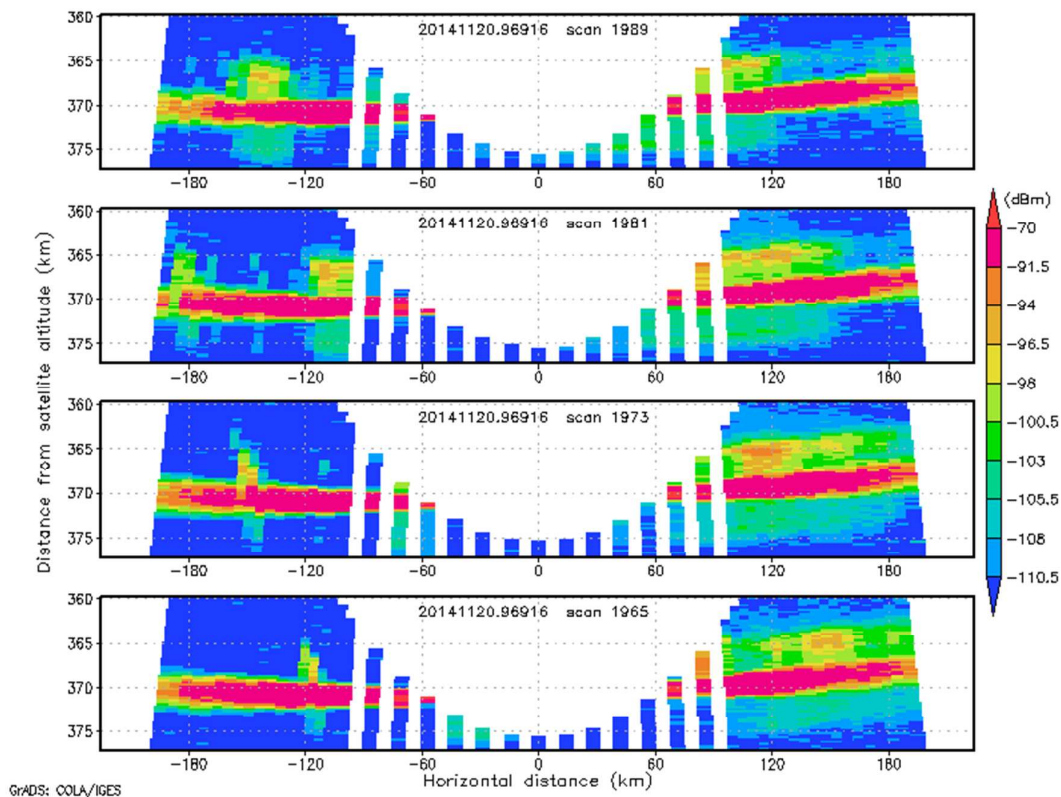
Fig. 6. Example of along-track vertical cross sections relative to the

earth's surface echo during the 90 degree yaw; interval between successive

images is eight scans (from bottom to top) on November 20, 2014. Note that

the very strong echo (red color) around the distance of 370 km is that from

the earth's surface.

24
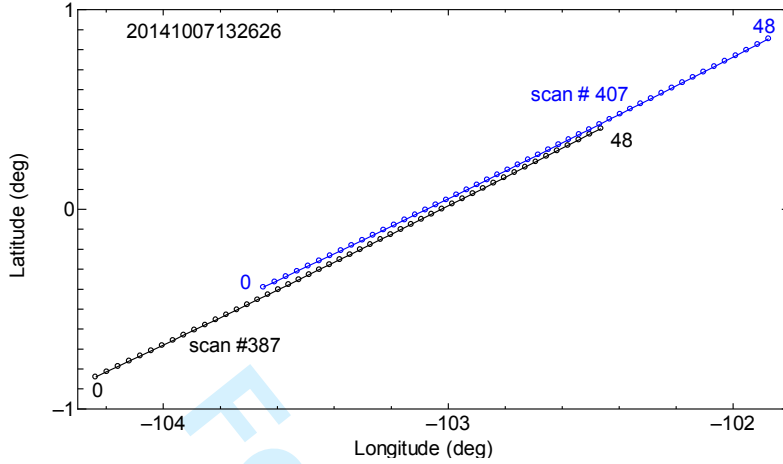
Fig. 7. Footprint location around the equator during the 90° yaw experiment.

In this figure, the footprint locations of two scans separated by 20 scan

intervals are shown.   The numbers near the circles indicate angle bin

numbers.   Data were taken during the 90° yaw test on October 7, 2014.

25
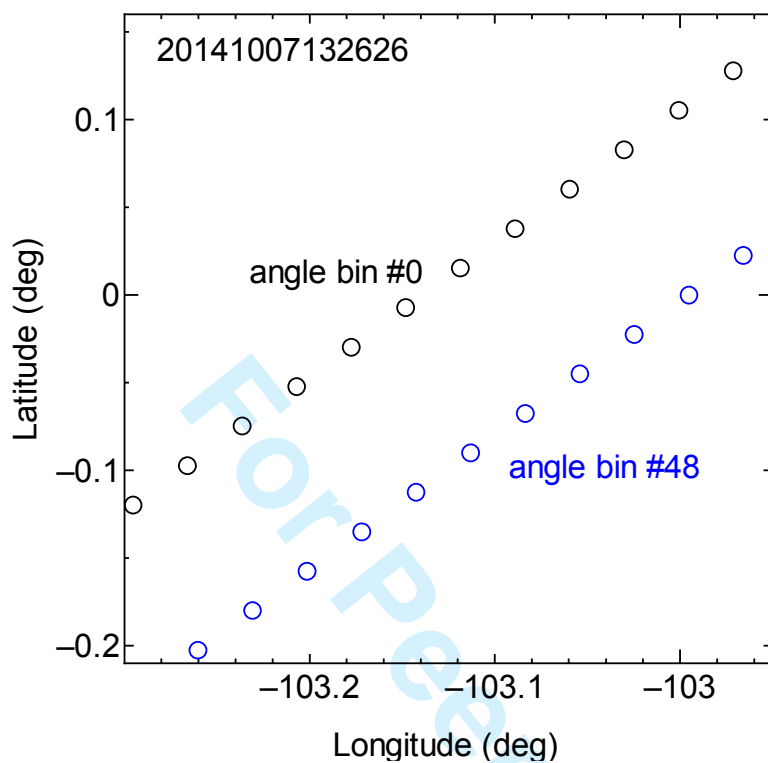
Fig. 8. Same as Fig. 7 except for the trajectories of the footprints of angle bin numbers 0 and 48.

26
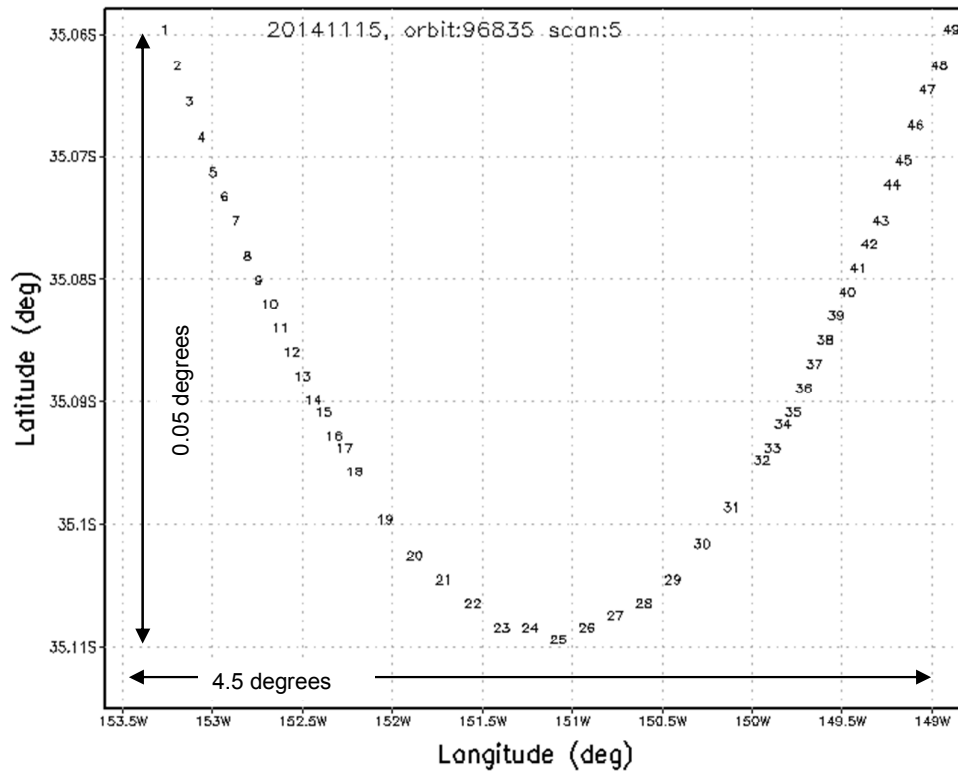
Fig. 9.   Example of the footprint location of one scan during the 90º yaw

experiment.   Note that the latitude range is about 0.05º whereas the

longitude range is about 5º.

27
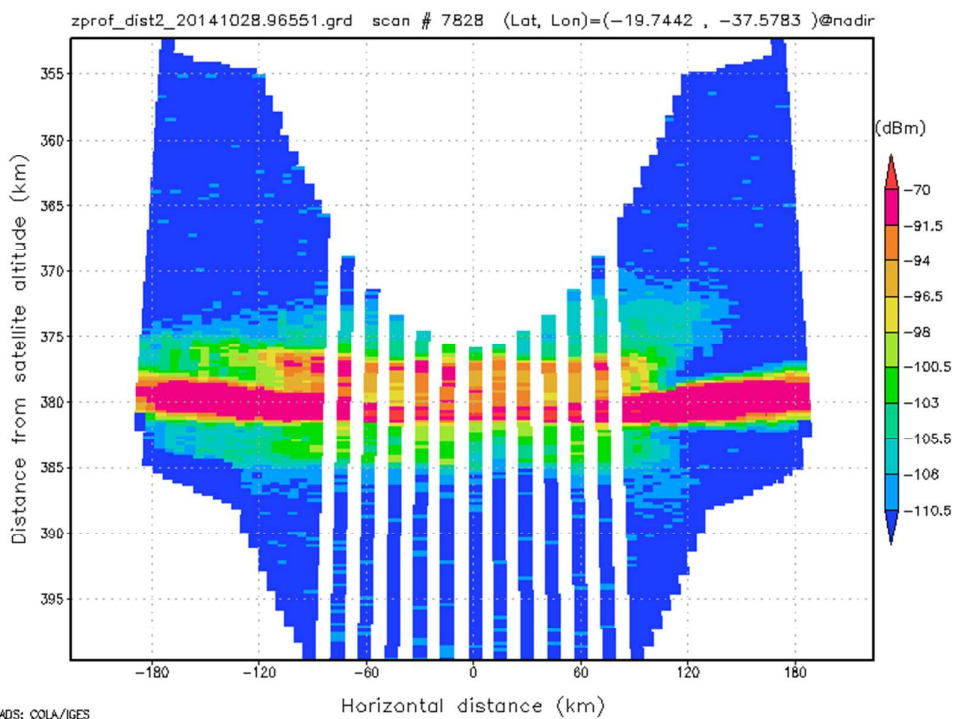
Fig. 10. Same as Fig. 6 but for the WS #1 experiment. Note that the very strong echo (red color) around the distance of 380 km is that from the earth's surface.

28
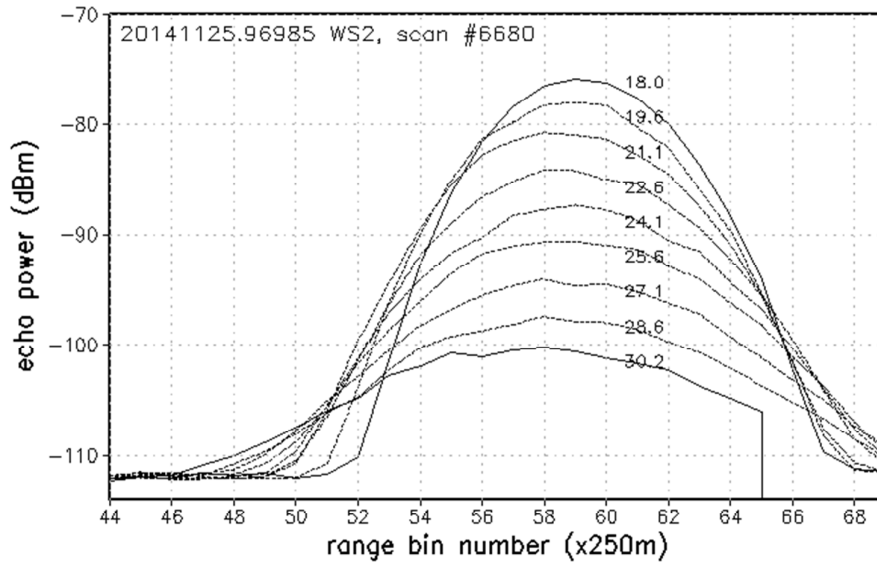
Fig. 11. Examples of the surface echo profile relative to the surface peak (around the range bin number of 60) during the Wide Swath #2 experiment from local zenith angles of 18.75° to 30.13°. Numbers in the figure indicate the local zenith angle in degrees.

29
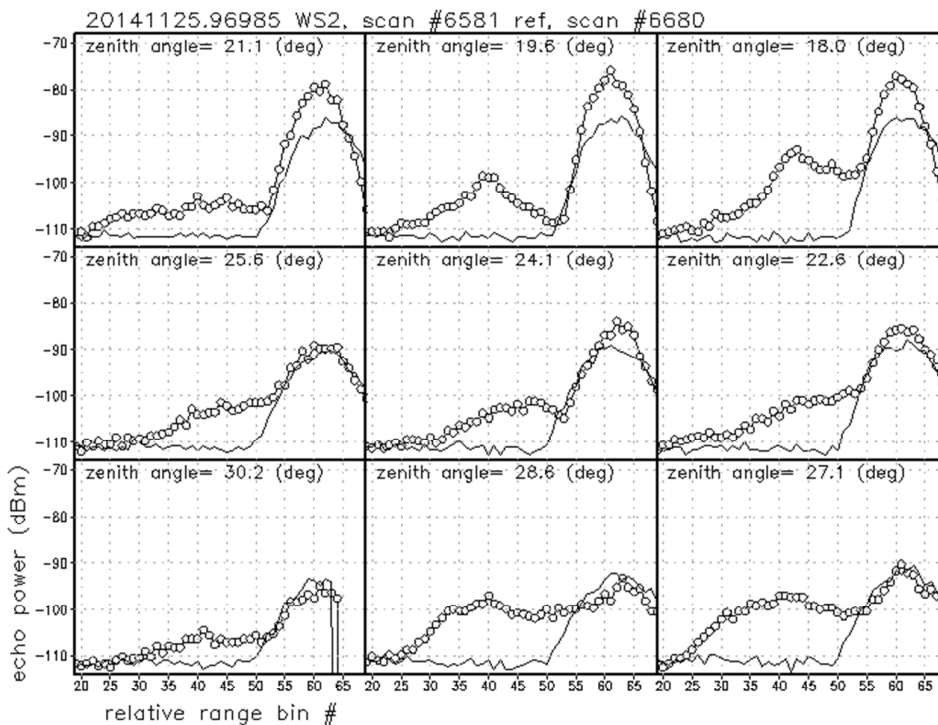
Fig. 12. Comparisons of near-surface echo profile relative to the earth's surface peak (around range bin number 60) in cases of rain (circles) and no rain (lines) for various incident angles (18.75° to 30.13° local zenith angles) wider than the scan edge of the normal scan.

30
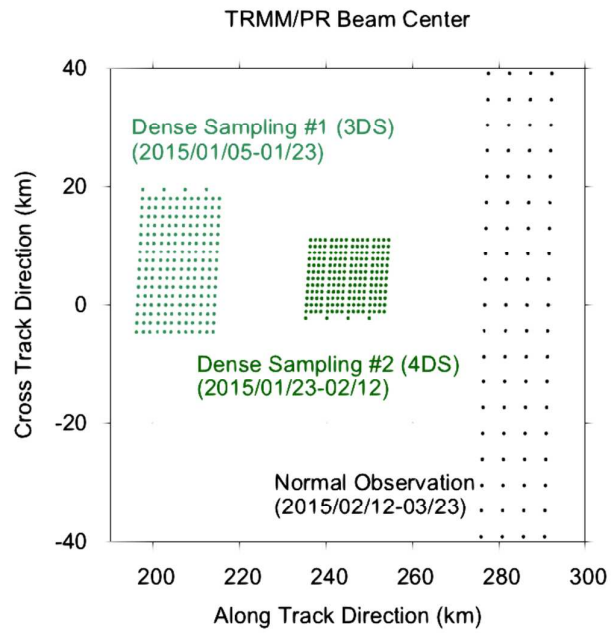
Fig. 13.　Scan geometry of the dense sampling experiment of the TRMM/PR

(left: 3 times dense sampling, middle 4 times dense sampling, right: normal

sampling) Note that each scan geometry shows the footprint of four scans.

31
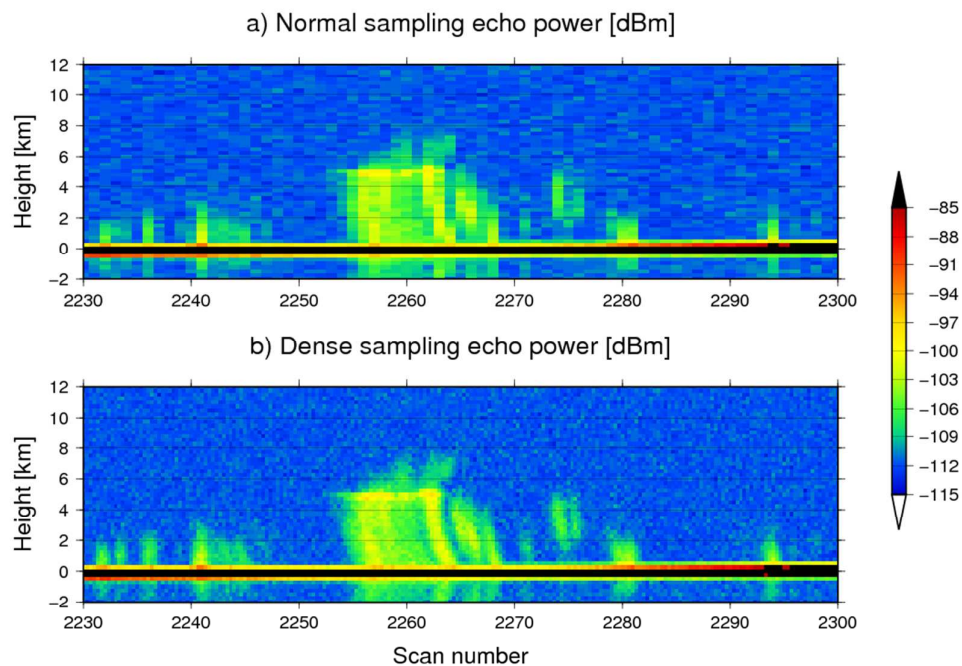
Fig. 14.   Example of the time-height cross section of the dense sampling

experiment (bottom).   For comparison, a normal sampling profile is shown

in the top panel.

32